Supplementary Material: Understanding the inter-model spread in global-mean hydrological sensitivity

Dagmar Fläschner* and Thorsten Mauritsen and Bjorn Stevens

Max Planck Institute for Meteorology, Hamburg, Germany

**Corresponding author address:* Atmosphere in the Earth System, Max Planck Institute for Meteorology, Bundesstraße 53, 20146 Hamburg, Germany

E-mail: dagmar.flaeschner@mpimet.mpg.de

S1. Temperature and water vapor kernels

Any interpretation of radiative decomposition of precipitation changes using the radiative kernel method depends on the applied kernel. The temperature kernel used in this study (Figure S1, left column) compares well with the one in Previdi (2010, Figure 1) in terms of magnitude and structure. However, differences are found in the longwave water vapor kernel (Previdi (2010, Figure 2) vs. Figure S1, middle column). In Previdi (2010), the longwave cooling due to water vapor increases from a 1 K warming at constant relative humidity is of similar magnitude in the lower troposphere as the longwave warming in the middle and upper troposphere. In the water vapor kernel used here, the lower-tropospheric cooling is larger than the warming by more than a factor of three. Here, the longwave (LW) component of η_{WV} enhances precipitation increase ($\eta_{\mathrm{WV,\,LW}} = -0.66 \pm 0.07\,\mathrm{W\,m^{-2}\,K^{-1}}$). The negative sign might arise because changes in water vapor in the lower troposphere are weighted more strongly and thus dominate the sign of the vertically integrated $\eta_{\mathrm{WV,\,LW}}$ contrary to Previdi (2010) who finds $\eta_{\mathrm{WV,\,LW}} = 0.29\,\mathrm{W\,m^{-2}\,K^{-1}}$. The values of the shortwave (SW) component of η_{WV} ($\eta_{\mathrm{WV,\,SW}} = 0.87 \pm 0.07\,\mathrm{W\,m^{-2}\,K^{-1}}$ here and $0.98\,\mathrm{W\,m^{-2}\,K^{-1}}$ in Previdi (2010)) are commensurate.

S2. Testing for influences on the adjustment residual

a. Non-linearity of ΔR_x with ΔT_s

The employed regression method assumes linear changes of ΔR_x with ΔT_{s}. The evolution of ΔR_x with ΔT_{s} is quasi-linear for most of the models and for all x besides ΔR_{LR} and ΔR_{WV} (not shown). The strongest non-linear behavior is found for the GFDL models in the lapse-rate and water vapor response, where the slope changes at approximately $\Delta T_{\mathrm{s}} = 2.5$ K (or after approximately 5 years). This issue extends to the estimates of the η decomposition. Nevertheless, the adjustment estimates are affected more strongly than the η decomposition as it relies on a good estimate of the slope during the beginning years of an abrupt forcing experiment; the estimate of the hydrological sensitivity parameter, however, is dominated by the weight of the remaining years. In fact, the GFDL models yield the lowest estimates of the lapse-rate adjustment (not shown) and thus represent the models with the greatest residual. The median of the adjustment residual does not strongly reduce when A_x are calculated from the regression over the first 10 years ($2.29\,\mathrm{W\,m^{-2}}$ vs. $2.50\,\mathrm{W\,m^{-2}}$). Even when excluding the GFDL models from the decomposition, the residual remains at $1.95\,\mathrm{W\,m^{-2}\,K^{-1}}$. The non-linearity does not appear to explain the offset of the residual.

b. Internal variability

To test whether the residual in the adjustment radiative decomposition arises because the regression method does not account for internal variability, we estimate the adjustment of the radiative atmospheric heat budget from CMIP5 fixed SST experiments, where sea surface temperatures are held fixed for a subset of *piControl* years (*sstClim*), and CO_2 concentrations are quadrupled (*sstClim4xCO2*). The change of the equilibrium mean radiative atmospheric fluxes gives the fast adjustment of precipitation (Hansen et al. 2005; Bala et al. 2010), which is then decomposed as described in Section 5a. Among other difficulties, this method features the disadvantage, that global mean $\Delta T_\mathrm{s} \neq 0$ due to land surface warming (Sherwood et al. 2015). We account for this additional warming by comparing the adjustments of the regression and fixed SST methods at the global mean ΔT_s found for the given model from the fixed SST experiment. The comparison is performed for the intersection of 12 available fixed SST and *abrupt4xCO2* models (BNU-ESM is excluded as it provides an unreasonably low global mean longwave surface emittance of $271.35\,\mathrm{W\,m^{-2}\,K^{-1}}$ for a mean surface temperature of 286.95 K).

Although the comparison of methods points out some differences for the decomposed adjustment, the offset in the residual is only slightly reduced (Figure S2). Differences in the surface albedo, Planck and water vapor adjustment will not appreciably modify the residual, because their values are small compared to the residual. The CO_2+Stratospheric temperature, cloud and sensible heat flux adjustment agree well among both methods. The lapse-rate adjustment is less negative in the fixed SST method, probably due to different land temperature changes in the fixed SST experiment. The less negative lapse-rate adjustment in the fixed SST method leads to a greater $\sum_x \Delta R_x$, and with that, contributes to the slightly reduced offset in the residual (medians of fixed SST and regression method are $1.27\,\mathrm{W\,m^{-2}}$ vs. $1.34\,\mathrm{W\,m^{-2}}$ for the subset of 12 models). It remains open, though, whether the different lapse-rate adjustment estimate is an indication that the regression method overestimates fast lapse-rate changes, or whether the actual fast lapse-rate changes are underestimated because the coupling between SST and the atmosphere is disabled in the *sstClim* experiments.

References

Bala, G., K. Caldeira, and R. Nemani, 2010: Fast versus slow response in climate change: implications for the global hydrological cycle. *Climate Dynamics*, **35 (2-3)**, 423–434, doi: 10.1007/s00382-009-0583-y, URL http://dx.doi.org/10.1007/s00382-009-0583-y.

Hansen, J., and Coauthors, 2005: Efficacy of climate forcings. *Journal of Geophysical Research: Atmospheres*, **110 (D18)**, n/a–n/a, doi:10.1029/2005JD005776, URL http://dx.doi.org/10.1029/2005JD005776.

Previdi, M., 2010: Radiative feedbacks on global precipitation. *Environmental Research Letters*, **5 (2)**, 025 211, URL http://stacks.iop.org/1748-9326/5/i=2/a=025211.

Sherwood, S. C., S. Bony, O. Boucher, C. Bretherton, P. M. Forster, J. M. Gregory, and B. Stevens, 2015: Adjustments in the Forcing-Feedback Framework for Understanding Climate Change. *Bull. Amer. Meteor. Soc.*, **96 (2)**, 217–228, doi:10.1175/BAMS-D-13-00167.1, URL http://dx.doi.org/10.1175/BAMS-D-13-00167.1.

LIST OF FIGURES

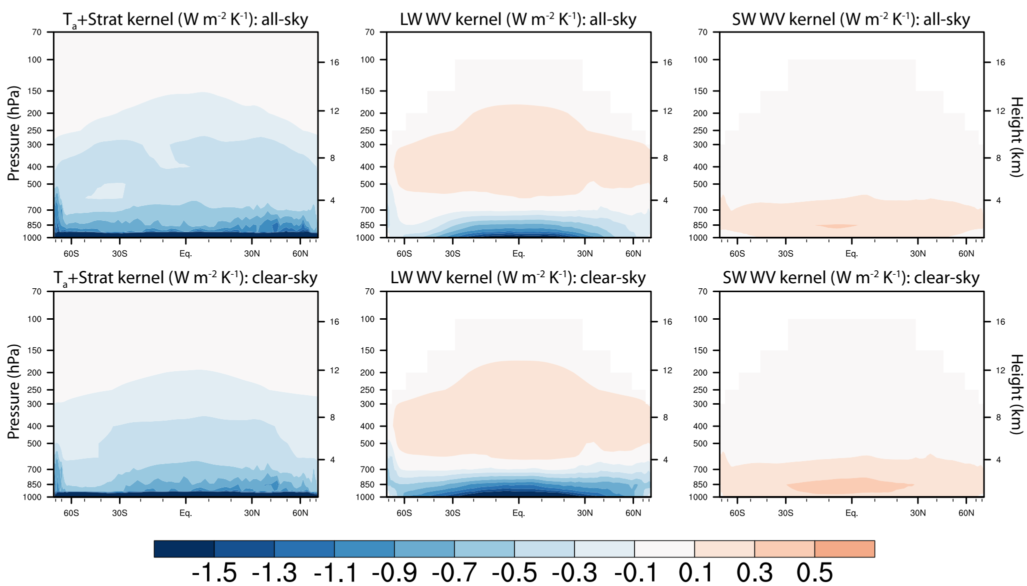

FIG. S1. Annual zonal mean temperature and water vapor kernels used for the radiative decomposition of precipitation change with warming in Section 5a. Atmospheric heating due to a uniform raise of atmospheric temperatures by 1 K (left), the heating of water vapor change due to a 1 K warming at constant relative humidity is separated into the longwave (middle) and shortwave (right) components. The all-sky (top) and clear-sky (bottom) are shown. Data is weighted by the depth of the corresponding pressure level.

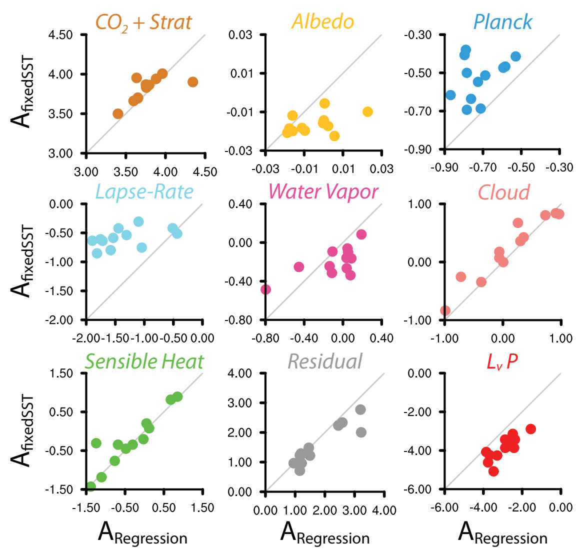

FIG. S2. Comparison of adjustment estimates with two calculation methods: regression method for *abrupt4xCO2* experiment and fixed-SST method for *sstClim4xCO2* experiment. Dots represent individual models. The line with a slope of one is shown in gray.